© 2019. Published by The Company of Biologists Ltd | Journal of Cell Science (2019) 132, jcs230748. doi:10.1242/jcs.230748

RESEARCH ARTICLE

Glucocorticoids delay RAF-induced senescence promoted by EGR1

Cyril Carvalho[1], Valentin L'Hôte[1], Régis Courbeyrette[1], Gueorgui Kratassiouk[1], Guillaume Pinna[1], Jean-Christophe Cintrat[2], Cyril Denby-Wilkes[1], Céline Derbois[3], Robert Olaso[3], Jean-François Deleuze[3], Carl Mann[1,*] and Jean-Yves Thuret[1,*]

ABSTRACT

Expression of hyperactive RAF kinases, such as the oncogenic B-RAF-V600E mutant, in normal human cells triggers a proliferative arrest that blocks tumor formation. We discovered that glucocorticoids delayed the entry into senescence induced by B-RAF-V600E in human fibroblasts, and allowed senescence bypass when the cells were regularly passaged, but that they did not allow proliferation of cells that were already senescent. Transcriptome and siRNA analyses revealed that the EGR1 gene is one target of glucocorticoid action. Transcription of the *EGR1* gene is activated by the RAF-MEK-ERK MAPK pathway and acts as a sensor of hyper-mitogenic pathway activity. The EGR1 transcription factor regulates the expression of p15 and p21 (encoded by *CDKN2B* and *CDKN1A*, respectively) that are redundantly required for the proliferative arrest of BJ fibroblasts upon expression of B-RAF-V600E. Our results highlight the need to evaluate the action of glucocorticoid on cancer progression in melanoma, thyroid and colon carcinoma in which B-RAF-V600E is a frequent oncogene, and cancers in which evasion from senescence has been shown.

KEY WORDS: Oncogene-induced senescence, B-RAF-V600E, EGR1, Glucocorticoid, CDKN1A, CDKN2B

INTRODUCTION

A remarkably high fraction (~50%) of melanomas express the oncogenic mutation B-RAF-V600E leading to constitutive activation of the B-RAF kinase (Shain et al., 2015). B-RAF-V600E is also a frequent oncogenic mutation in thyroid and colorectal cancers (Cantwell-Dorris et al., 2011). However, expression of this driver mutation in normal human fibroblasts or melanocytes triggers premature senescence and thus blocks progression to a tumor (Damsky and Bosenberg, 2017; Shain et al., 2015). This finding suggests that the proliferative arrest induced by the expression of hyper-active RAF kinases in normal cells acts as a suppressor mechanism that must be bypassed if a tumor is to be formed. The molecular mechanisms responsible for RAF-induced senescence are poorly defined. Increased expression of the p21, p16 and p15 (also known as CDKN1A, CDKN2A and CDKN2B, respectively) cyclin-dependent kinase inhibitors have been implicated in this proliferative arrest to different extents depending on the investigated model, but the pathways leading to derepression of the corresponding genes are incompletely understood (Jeanblanc et al., 2012; McNeal et al., 2015; Michaloglou et al., 2005; Woods et al., 1997; Zhu et al., 1998). Senescence induced by the RAS-val12 oncogene has been studied in greater detail. In response to mitogenic factors binding to cell surface receptors, RAS activates several growth-promoting pathways including the RAF-MEK-ERK, PI3K and Ral GTPase pathways (Fey et al., 2016). Expression of RAS-val12 has been shown to induce a replicative stress that is a major factor in triggering proliferative arrest (Di Micco et al., 2006), but DNA damage does not appear to be necessary for senescence induced by RAF (Damsky and Bosenberg, 2017; Jeanblanc et al., 2012). Hyperactivation of the RAF-MEK-ERK pathway may trigger proliferative arrest through specific signaling pathways. We screened a library of clinically approved molecules and discovered that glucocorticoids are potent modulators of RAF-induced senescence in human fibroblasts. Glucocorticoids are widely used as anti-inflammatory agents in the clinic, but activation of the glucocorticoid receptor NR3C1 by binding of glucocorticoids leads to the rapid activation and repression of hundreds of genes implicated in diverse pathways in a cell-specific manner (Sacta et al., 2016; Weikum et al., 2017). Transcriptomic analysis identified the *EGR1* gene as a candidate target of glucocorticoids. Loss of function experiments for EGR1 and ChIP-seq analyses suggest that the transcription factor EGR1 acts as a sensor of MAPK hyperactivity contributing to the triggering of senescence.

RESULTS

Glucocorticoids delay or bypass entry into oncogene-induced senescence

We screened the Prestwick drug repositioning library for molecules that could inhibit senescence of WI-38hTert human fibroblasts induced by the expression of an activated form of the C-RAF kinase that we previously characterized (Jeanblanc et al., 2012). 26 different glucocorticoids inhibited RAF-induced senescence in this screen (see Materials and Methods). In addition, previous work by Cristofalo and colleagues has shown that glucocorticoids can delay replicative senescence of human fibroblasts (Mawal-Dewan et al., 2003) and Laberge et al. have recently shown that glucocorticoids partially inhibit the senescence-associated secretory phenotype (SASP) of fibroblasts induced into senescence by RAS-val12 (Laberge et al., 2012). We therefore set out to describe and analyze effects of glucocorticoids on RAF-induced senescence. To this end, and to study the effects of glucocorticoids on senescence induced by a mutation relevant for human oncogenesis, we developed a new cellular model of BJhTert human foreskin fibroblasts where the expression of B-RAF-V600E is under the control of a doxycycline responsive tet-ON promoter.

[1]Institute for Integrative Biology of the Cell (I2BC), CEA, CNRS, Univ. Paris-Sud, Université Paris-Saclay, 91198 Gif-sur-Yvette cedex, France. [2]Service de Chimie Bio-organique et Marquage (SCBM), CEA, Université Paris-Saclay, 91191 Gif-sur-Yvette, France. [3]Centre National de Recherche en Génomique Humaine (CNRGH), Institut de Biologie François Jacob, CEA, Université Paris-Saclay, F-91057 Evry, France.

*Authors for correspondence (carl.mann@cea.fr; jean-yves.thuret@cea.fr)

V.L., 0000-0001-5168-2943; J.-Y.T., 0000-0001-5385-7620

Received 13 February 2019; Accepted 22 July 2019

Journal of Cell Science (2019) 132, jcs230748. doi:10.1242/jcs.230748

Oncogene-induced senescence (OIS) is known to occur independently of hTert expression and allowed us to study this senescence in the absence of possible confounding contributions due to the loss of telomeric sequences in non-immortalized fibroblasts (Jeanblanc et al., 2012; Wei and Sedivy, 1999). In our model, the concentration of doxycycline controls the expression of B-RAF-V600E at the mRNA and protein levels (Fig. 1A,B). The expression of B-RAF-V600E at low levels of doxycycline (in the range of 5–20 ng ml^{-1} depending on the experiment) is, on average, similar to the endogenous level of B-RAF (Fig. 1B; Fig. S1G).

We then assessed the effect of B-RAF-V600E expression levels on proliferation. Cell numbers decreased with increasing concentrations of doxycycline over 5 days of culture (Fig. 1C). The doxycycline concentration for which the number of cells starts declining is similar to the concentration at which the expression of B-RAF-V600E is close to endogenous levels. Greater than 80% of cells lost the ability to go through S-phase within the first 24 h in high (1000 ng ml^{-1}) concentrations of doxycycline (Fig. 1D). The proliferation arrest was slower at lower concentrations of doxycycline (100 ng ml^{-1}, orange; 50 ng ml^{-1}, blue). To take advantage of the fast proliferative arrest in order to investigate mechanisms, all further experiments were carried out at 1000 ng ml^{-1} doxycycline unless indicated otherwise. As expected, in addition to cell cycle arrest, the expression of B-RAF-V600E led to increased senescence-associated (SA)-β-galactosidase activity (Fig. 1E), the formation of senescence-associated heterochromatic foci (SAHFs, Fig. 1F), and the derepression of cyclin-dependent kinase inhibitors (see below) as typical senescence markers.

To assess the effects of glucocorticoids on senescence induction, we then incubated the cells with clobetasol, a potent glucocorticoid used in topical applications to treat inflammatory skin diseases. Within the timeframe of the experiment (5 days), low nanomolar levels of clobetasol strongly inhibited the proliferative arrest of BJ cells induced by B-RAF-V600E (Fig. 2A). All further experiments were carried out at 2 nM clobetasol. We also observed delays in proliferative arrest after induction of an activated C-RAF kinase in BJ cells (with cortisol, Fig. S1A, and clobetasol, Fig. S1C) and WI-38 cells (with clobetasol, Fig. S1B), and also in IMR-90 cells expressing RAS-val12 (with clobetasol, Fig. S1D). Glucocorticoids can thus interfere with the proliferative arrest induced by both activated RAF and RAS oncogenes in three different fibroblast cell lines.

Clobetasol treatment allowed BJ cells expressing high levels of B-RAF-V600E to maintain significant DNA synthesis for at least 5 days (Fig. 2B, green). Proliferation was assayed in 96-well plates (see Materials and Methods). In this microwell assay, we cannot determine whether the reduced DNA synthesis beginning at 3 days is due to delayed entry into senescence in the presence of clobetasol or whether it is due to contact inhibition of proliferation as cells approach confluence. We followed proliferation in continuous cultures to determine the long-term effects of clobetasol on RAF-induced senescence. Remarkably, incubation of cells with clobetasol at low or high doxycycline concentration allowed full bypass of senescence when the cells were passaged every 2 days (Fig. 2C). Surprisingly, when cells expressing B-RAF-V600E were not passaged, the presence of clobetasol delayed, but did not lead to a bypass of the senescence proliferative arrest (Fig. 2D; Fig. S1E). Similar results were observed in clonogenic assays (Fig. S1H). Low levels of doxycycline (15 or 30 ng ml^{-1}) blocked the ability of BJ cells to form colonies on plates, but colonies were restored in the presence of clobetasol. However, clobetasol did not allow colony

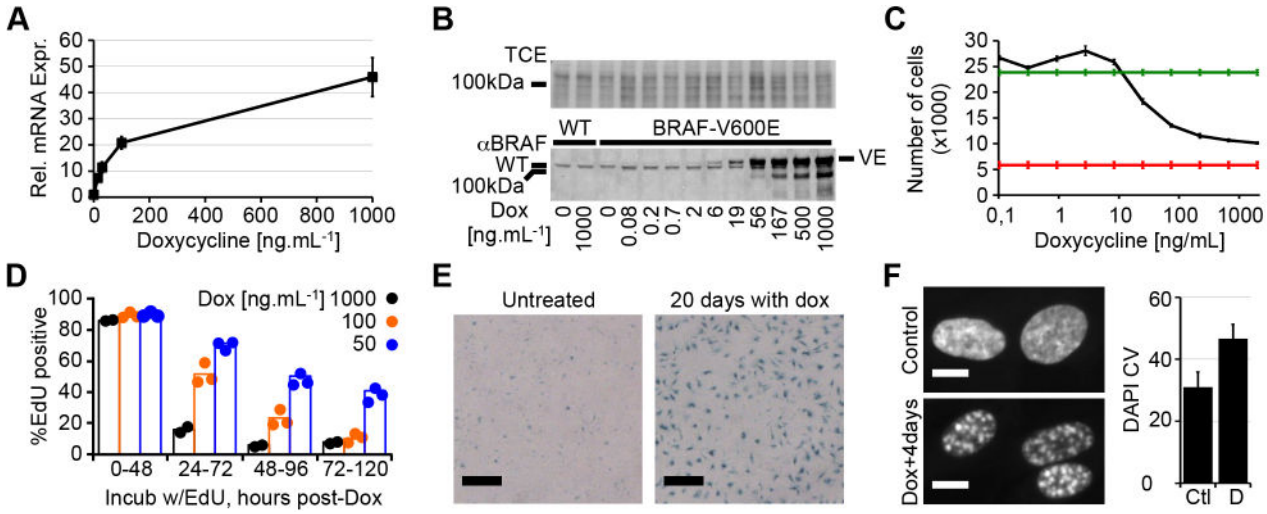

Fig. 1. Rapid Induction of senescence with inducible B-RAF-V600E. (A) Relative RNA expression as determined by RT-qPCR of B-RAF-V600E cells with increasing doxycycline concentrations and 24 h incubation normalized to the expression with ethanol (dox=0) (error bars s.d.). A representative experiment from two biological repeats each with *n*=3 is shown. (B) Representative anti-B-RAF western blot on whole-cell extracts of BJhTert cells (WT) or BJhTert cells transduced with a pTRIPz-3HA-B-RAF-V600E lentivirus (B-RAF-V600E). Cells were harvested 48 h after inducing with increasing doxycycline concentrations. WT also indicates the endogenous B-RAF protein and VE indicates the B-RAF-V600E construct that has three N-terminal tandem hemagglutinin (HA) epitopes and migrates slightly slower than the endogenous protein. A portion of the gel stained with 2,2,2-trichloroethanol (TCE) is shown as a loading control for total protein. (C) Number of cells after culture with increasing doxycycline concentrations for 5 days. Green line: maximum number of cells obtained by culture with ethanol solvent control. Red line: minimum number of cells obtained by plating with medium containing 20 µM etoposide instead of doxycycline. This level of etoposide rapidly blocks proliferation through acute DNA damage. A representative experiment from three biological repeats each with *n*=3 is shown. Error bars show the s.d. (D) Percentage of cells going through S-phase during a 48-h sliding window at the indicated times after doxycycline addition at the indicated concentrations. A representative experiment from three biological repeats each with *n*=3 is shown. (E) Representative SA-β-galactosidase staining of proliferative cells (Untreated) and cells incubated for 20 days with 1000 ng ml^{-1} doxycycline. Scale bars: 400 µm. (F) Left panels, representative images of DAPI-stained nuclei to visualize DNA compaction in proliferating cells (Control) and in cells treated with 1000 ng ml^{-1} doxycycline for 4 days. Scale bars: 10 µm. Right panel, measure of chromatin compaction {DAPI CV, coefficient of variation of DAPI intensity [standard deviation as a percentage of the mean (Contrepois et al., 2012)]} in untreated proliferating control cells (Ctl) versus cells incubated for 4 days with 1000 ng ml^{-1} doxycycline (D). A representative experiment from two biological repeats each with *n*=3 is shown. Error bars show s.d.

Journal of Cell Science

Journal of Cell Science (2019) 132, jcs230748. doi:10.1242/jcs.230748

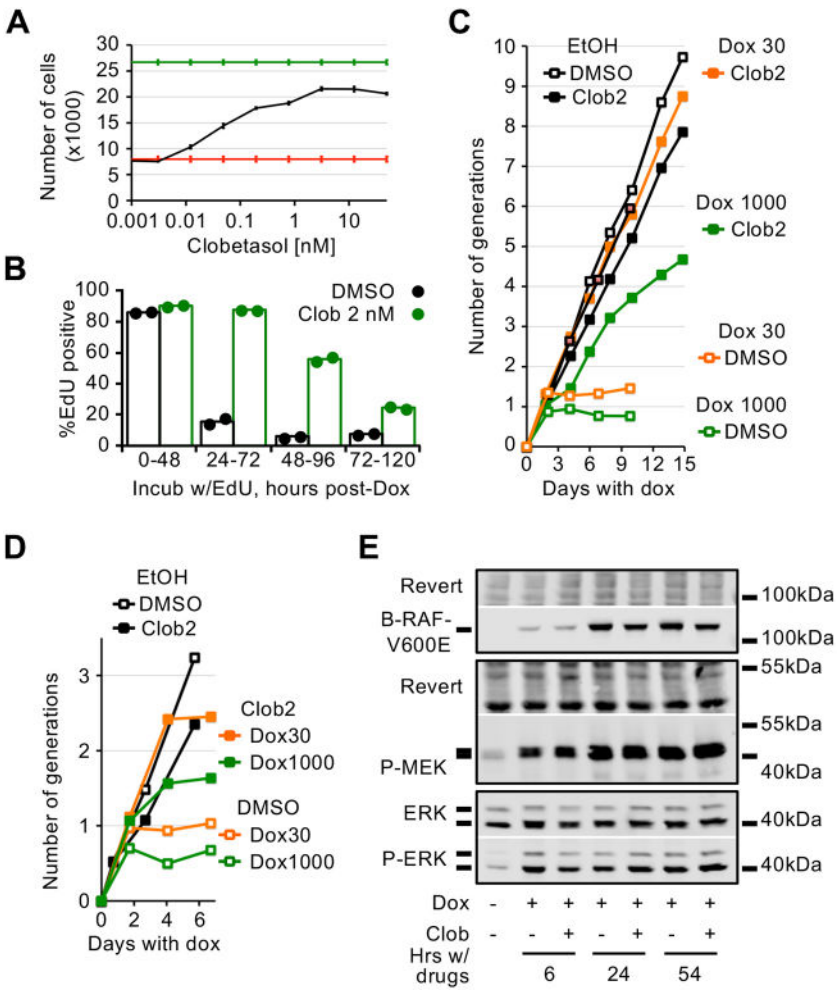

Fig. 2. Clobetasol interferes with senescence onset without interfering with MAPK activation. (A) Number of cells after culture with 1000 ng ml^{-1} doxycycline and increasing clobetasol concentrations for 5 days. Green line: culture with ethanol (vehicle for doxycycline) and DMSO (vehicle for clobetasol). Red line: culture with etoposide (20 µM). A representative experiment from three biological repeats each with *n*=3 is shown. Error bars show s.d. (B) Percentage of cells going through S-phase during a 48-h sliding window at the indicated times after 1000 ng ml^{-1} doxycycline addition with 2 nM clobetasol (green) or DMSO (black). A representative experiment from three biological repeats each with *n*=3 is shown. (C) Number of cumulative generations. Cells were systematically passaged every 2–3 days with the indicated drugs and counted. A representative experiment from two biological repeats each with *n*=3 is shown. Doxycycline (Dox) concentrations in ng ml^{-1}, clobetasol (Clob) in nM. (D) Number of cumulative generations as in panel C with the difference that cells were not passaged. Cells counted (then discarded) from successive plates prepared at day 0 and kept in identical conditions, except for EtOH-treated cells that had to be passaged at confluency. A representative experiment from two biological repeats each with *n*=3 is shown. The remaining cultures had undergone proliferative arrest before confluency. Doxycycline (Dox) concentrations in ng ml^{-1}, clobetasol (Clob) in nM. (E) Representative western blots (*n*=4) on whole-cell extracts. 3HA-B-RAF-V600E was detected with an anti-B-RAF antibody. ERK1/2 (ERK) and phospho-ERK1/2 (P-ERK) were detected on the same gel with 700 nm and 800 nm fluorescent secondary antibodies. ERK2 is the strong band at 40 kDa and ERK1 is the weaker band that migrates at a slightly higher molecular mass. P-MEK is phospho-MEK1/2. Portions of the membranes stained with the Revert protein stain (Li-Cor) are shown as loading controls.

formation when BJ cells were plated in the presence of 1000 ng ml^{-1} doxycycline. Collectively, these results suggest that an irreversible proliferative arrest results from the integration of positive (glucocorticoid signaling, frequent cell passing and renewal of nutrients) and negative proliferative signals (hyperactive RAF kinase signaling, contact inhibition and stress associated with high cell dilution on plates for clonogenicity assays).

We conclude from these experiments that B-RAF-V600E triggers senescence in human BJ fibroblasts when the oncogene is expressed at levels similar to the endogenous kinase, but the cell cycle arrest is faster at high expression levels of B-RAF-V600E. Glucocorticoids allow the cells to fully bypass senescence, even at high levels of oncogene expression, when regularly passaged in the absence of exogenous stress. In contrast, once senescent, BJ cells did not resume proliferation when treated with clobetasol (Fig. 2D; Fig. S1E,F). Thus, clobetasol delays or bypasses entry into senescence, but does not revert the established senescent state. We therefore set out to identify the mechanisms involved in senescence induced by B-RAF-V600E and modulated by glucocorticoids. In all subsequent experiments, cells were not passaged after doxycycline addition unless indicated.

Identification of glucocorticoid targets in senescence induction

Glucocorticoids are steroid hormones that function by binding to the glucocorticoid receptor (GR, encoded by the *NR3C1* gene), which then activates or represses target genes after translocation to the nucleus (Sacta et al., 2016; Weikum et al., 2017). The GR was located in both the cytosol and nucleus of BJ cells in proliferation or after B-RAF-V600E expression, but treatment with 2 nM clobetasol resulted in a rapid increase in nuclear GR (Fig. S2A,B). The effects of clobetasol on senescence induction were dependent on the GR, as depleting *NR3C1* mRNA fully abolished the effect of clobetasol on proliferation (Fig. S2C), and RU-486, which antagonizes the activation of the GR by glucocorticoids (Cadepond et al., 1997), also blocked the effect of clobetasol on proliferation (Fig. S2D). We next sought to determine how activated GR suppresses RAF-induced senescence. Clobetasol treatment did not interfere with the induction of B-RAF-V600E or the phosphorylation of MEK1 and MEK2 (MEK1/2, also known as MAP2K1 and MAP2K2, respectively) or ERK1 and ERK2 (ERK1/2, also known as MAPK3 and MAPK1, respectively) (Fig. 2E), so glucocorticoids must work downstream of ERK1/2 hyperactivation to suppress senescence.

GR-mediated antagonism of transcription factors such as NF-κB explains its anti-inflammatory action, and NF-kB (RelA subunit)-mediated expression of inflammatory factors has been implicated in contributing to senescence induction in some systems (Chien et al., 2011). We first tested a role for NF-κB in RAF-induced proliferative arrest by constructing a version of our BJhTert/ptet-ON-B-RAF-V600E cell line that expresses the IκB-SR (super repressor), a mutant version of IκB that acts as a dominant-negative suppressor of NF-κB by sequestering RelA in the cytoplasm (Karin and Ben-Neriah, 2000). Treatment of parental cells with TNF led to

Journal of Cell Science (2019) 132, jcs230748. doi:10.1242/jcs.230748

a rapid nuclear translocation of RelA, whereas RelA remained cytosolic after treatment of the IκB-SR-expressing cell line with TNF (Fig. S3A). Notably, expression of B-RAF-V600E triggered the proliferative arrest of these IκB-SR-expressing cell lines to a similar degree to that seen in the parental cell line (Fig. 3A), and clobetasol treatment interfered with this proliferative arrest as in the parental cell line (Fig. 3B). Thus, RelA transcriptional activity is not required for the RAF-induced proliferative arrest, or for clobetasol modulation of this proliferative arrest.

We further tested a possible role for the repression of inflammatory gene expression on the suppression of RAF-induced senescence by characterizing the effect of compound A (CpdA). Long-term treatment with glucocorticoids in the clinic produces adverse side effects that are thought to be due to the transcriptional activation of multiple genes by the GR. CpdA, a non-steroidal plant-derived compound, was identified as a molecule that could block NF-κB-driven gene expression without transcriptionally activating genes that could be responsible for the unwanted side effects of the GR (Lesovaya et al., 2015). We found no effect of CpdA on senescence induced by the expression of B-RAF-V600E (Fig. S3B), despite the existence of a transcriptional response partially overlapping the response to clobetasol (Fig. S3C). This result supports our conclusion that the repression of inflammatory gene expression by glucocorticoids is not required for their action in bypassing RAF-induced senescence.

Having excluded inflammatory gene repression in the senescence bypass by clobetasol, we next used transcriptome analyses to identify candidate gene targets. Since we had observed that cell cycle arrest was almost complete 24 h after doxycycline addition (1000 ng ml^{-1}), that clobetasol was active during that period of time and that CpdA had no effect on senescence induction, we reasoned that good candidate genes would have the following characteristics: (1) be induced or repressed with 24 h of doxycycline treatment compared to non-treated cells, (2) be differentially expressed upon clobetasol treatment (opposing the effect of doxycycline), and (3) not be affected by CpdA. Furthermore, as we sought direct targets of glucocorticoid, we chose a short treatment of 2 h with clobetasol or CpdA after 24 h of incubation with doxycycline. As shown in Fig. 3C, we found a limited number of candidate Illumina microarray probes with such characteristics [at a false discovery rate (FDR)<1×10^{-4}, 17 upregulated and 45 downregulated, corresponding to 14 distinct upregulated genes and 39 distinct downregulated genes].

In parallel to this study, we also performed an siRNA screen to identify chromatin-associated or signaling proteins required for RAF-induced senescence. EGR1, which is a candidate glucocorticoid-target gene as defined above (Fig. 3C), was among the genes targeted in this screening. Interestingly, knockdown of EGR1 allowed cells to divide more during the first 4 days of oncogene expression (Fig. S4). The early growth response-1 (*EGR1*) gene encodes a transcription factor, and the expression of the *EGR1* gene is directly controlled by the MAPK pathway (Bahrami and Drabløs, 2016). We thus decided to focus on its role in senescence induction and the response to glucocorticoids.

EGR1 and the cell cycle arrest during senescence induction

EGR1 has three homologs in the human genome (EGR2–EGR4). EGR3 (but not EGR2 and EGR4) was also identified as a possible glucocorticoid target during senescence induction (Fig. 3C; Fig. S5A). As shown in Fig. 4A, treatment of cells with an anti-EGR1 siRNA (different from the siRNA used in Fig. S4), but not with two anti-EGR3 siRNAs, allowed more proliferation after

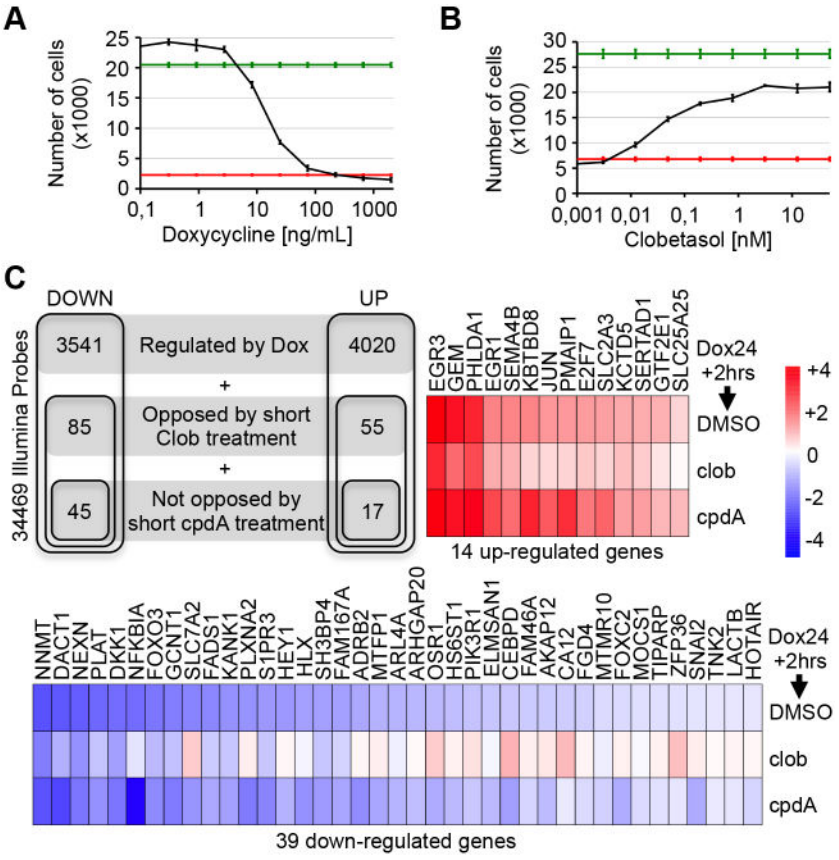

Fig. 3. Senescence suppression by clobetasol does not require RelA, and transcriptomics analysis identifies candidate target genes. (A) Number of IκB-SR-expressing cells after culture with increasing doxycycline concentrations for 5 days. Green line: culture with ethanol (vehicle for doxycycline). Red line: culture with etoposide (20 μM). A representative experiment from two biological repeats each with *n*=3 is shown. Error bars show s.d. (B) Number of IκB-SR-expressing cells after culture with 1000 ng ml^{-1} doxycycline and increasing clobetasol concentrations for 5 days. Green line: culture with ethanol and DMSO (vehicles for doxycycline and clobetasol). Red line: culture with etoposide (20 μM). A representative experiment from two biological repeats each with *n*=3 is shown. Error bars show s.d. (C) Transcriptomics analysis using Illumina beadarray data. Upper left panel: number of up- and down-regulated probes (FDR<1×10^{-4}) between cells treated with ethanol and DMSO (proliferative) and cells treated with 1000 ng ml^{-1} doxycycline for 24 h, with successive filters for differential expression after short (2 h) clobetasol treatment and the absence of response to short compound A treatment. Note that some genes were represented by two different probes so that the 17 upregulated probes and 45 downregulated probes corresponded to only 14 distinct upregulated genes and 39 distinct downregulated genes. Other panels: for probes corresponding to the indicated genes, the log2(Fold Change) between proliferative cells and cells incubated for 24 h with 1000 ng ml^{-1} doxycycline and 2 h with DMSO, clobetasol (2 nM) or compound A (2 μM, see Fig. S3B) is shown as a color representation, with blue indicating downregulation and red upregulation.

Journal of Cell Science (2019) 132, jcs230748. doi:10.1242/jcs.230748

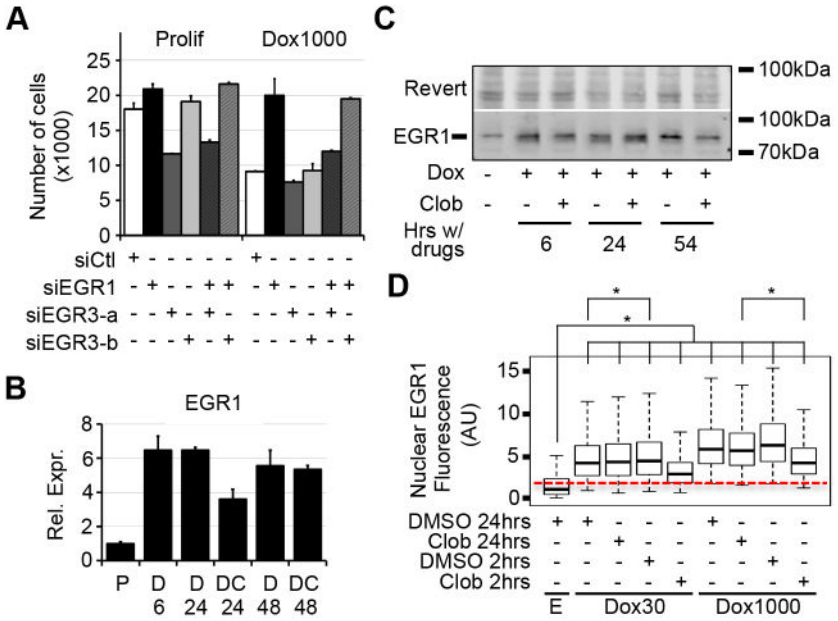

Fig. 4. EGR1 is a target of clobetasol rapidly induced after B-RAF-V600E expression, and its knockdown delays proliferation arrest. (A) Number of cells after treatment with the indicated siRNAs for 24 h, then incubation with ethanol (Prolif) or 1000 ng ml^{-1} doxycycline (Dox1000) for 96 h. A representative experiment from three biological repeats each with n=3 is shown. Error bars show s.d. (B) A representative experiment from two biological repeats each with n=3, showing the relative expression of EGR1 determined by RT-qPCR, and normalized to the expression level in P (ethanol) and DMSO at 24 h. D6, D24, D48, doxycycline (1000 ng ml^{-1}) and DMSO for 6, 24 or 48 h; DC24, DC48, doxycycline (1000 ng ml^{-1}) and clobetasol (2 nM) for 24 or 48 h. Error bars show s.d. (C) Representative western blot (n=3) of EGR1 expression at indicated times after doxycycline (1000 ng ml^{-1}) and DMSO or clobetasol (2 nM). A portion of the membrane stained with Revert protein stain (Li-Cor) is shown as a loading control. (D) Boxplots showing the integrated nuclear fluorescence (AU, arbitrary units) after anti-EGR1 immunostaining, with the median (thick line), first and third quartiles (lower and upper hinges) and whiskers extending to values 1.5 times the interquartile range. E, ethanol, Dox30, Dox1000, doxycycline 30 at 1000 ng ml^{-1} for 24 h. DMSO or clobetasol were either added at the same time as doxycycline (24 hrs) or 2 h before fixation with formaldehyde (2 hrs). The red dotted line indicates the intensity threshold for which 37% of cells were determined positive for nuclear EGR1. The asterisk indicates $P<2.2\times10^{-16}$ in a double-sided Kolmogorov–Smirnov test. A representative experiment from two biological repeats each with n=3 is shown.

BRAF-V600E induction. We thus excluded EGR3 from further consideration.

EGR1 RNA was significantly induced as soon as 6 h after doxycycline addition (Fig. 4B) and plateaued thereafter. Continuous treatment with clobetasol partially repressed EGR1 RNA induction at 24 h (Fig. 4B), but not 48 h after doxycycline addition. EGR1 protein levels increased at 6 h after doxycycline addition, and the simultaneous addition of doxycycline plus clobetasol had little effect on EGR1 protein levels (Fig. 4C). We then estimated the levels of EGR1 in individual cells through immunofluorescence staining. About a third (37%) of proliferating cells stained positively for EGR1 (Fig. S6), but almost all cells stained positively for EGR1 after incubating with low or high concentrations of doxycycline for 24 h (Fig. S6; Fig. 4D). Additionally, whereas a short treatment (2 h) with clobetasol resulted in a significant decrease in EGR1 levels, a continuous treatment with clobetasol did not (Fig. 4D). Thus, modulation of EGR1 protein levels by clobetasol is unlikely to explain all of the effects of clobetasol on the proliferative arrest.

EGR1 was previously implicated in cyclin-dependent kinase inhibitor (CKI) expression in different experimental contexts (Besancenot et al., 2010; Krones-Herzig et al., 2003; Salotti et al., 2015), and CKI accumulation is required for the proliferative arrest in senescence (Beausejour et al., 2003; Jeanblanc et al., 2012). We thus tested whether EGR1 contributes to CKI expression in our model. First, we identified the CKIs relevant to B-RAF-V600E-induced senescence in BJ fibroblasts. As shown in Table S1, at least one probe for CDKN1A, CDKN2A and CDKN2B showed significant induction 24 h after doxycycline addition in Beadarray transcriptomics experiments. RT-qPCR experiments confirmed that *CDKN1A*, *CDKN2A* and *CDKN2B* mRNA levels were upregulated after doxycycline addition (Fig. 5A), as were the corresponding p15, p16 and p21 protein levels (Fig. 5B). Interestingly, whereas *CDKN1A* and *CDKN2B* were not differentially expressed after short clobetasol treatments (2 h, Table S2), and accordingly were not identified as putative clobetasol targets, they were downregulated at the mRNA level during continuous 24 and 48 h clobetasol treatments (Fig. 5A). Levels of p15 and p21 proteins were also reduced (Fig. 5B). *CDKN2A* mRNA and protein levels were not decreased by short or long clobetasol treatments (Fig. 5A,B; Table S2).

We then assessed the effects of p21, p16 and p15 depletion on the proliferative arrest induced by the expression of B-RAF-V600E. Depletion of p16 had no effect on the proliferative arrest, whereas depletion of p21, and, to a lesser extent, p15, increased proliferation (Fig. 5C and Fig. S7A,B). Interestingly, combined depletion of p21 and p15 allowed more proliferation than either individual depletion, and yielded similar or better effects than the depletion of EGR1 (Fig. 5C). We then used siRNA to knockdown EGR1 in BJ cells and observed decreased expression of *CDKN1A* and *CDKN2B* in response to B-RAF-V600E expression (Fig. 6). Furthermore, ChIP-seq experiments revealed a significant increase of EGR1 occupancy at consensus EGR1-binding sites within the promoter of the *CDKN2B* gene and within the first intron of the *CDKN1A* gene upon expression of B-RAF-V600E (Fig. 7). From these experiments, we conclude that although p15, p16 and p21 are induced in response to B-RAF-V600E, only p15 and p21 play an important, partially redundant, role in the proliferative arrest in this cell line. Moreover, *CDKN1A* and *CDKN2B*, but not *CDKN2A*, are repressed by

Journal of Cell Science (2019) 132, jcs230748. doi:10.1242/jcs.230748

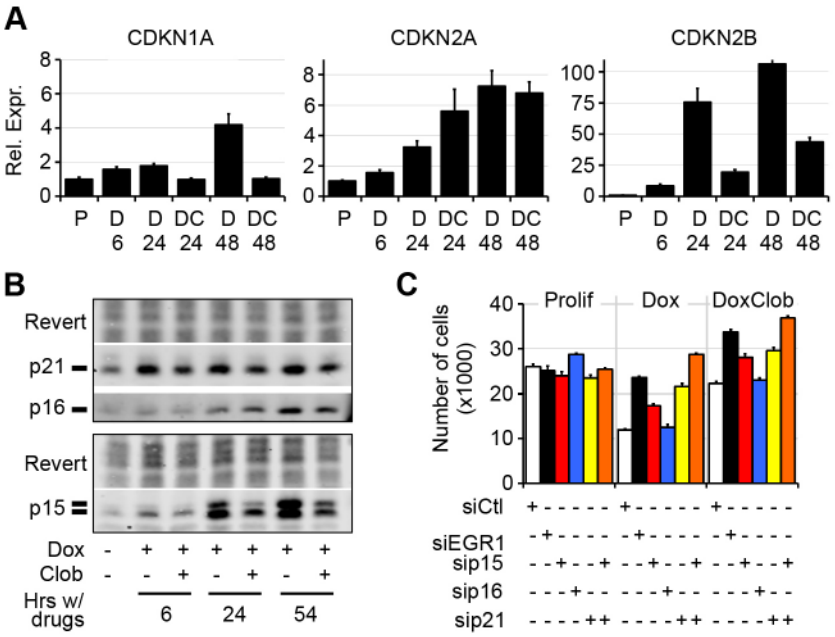

Fig. 5. p21-CDKN1A and p15-CDKN2B are involved in the proliferation arrest triggered by B-RAF-V600E, and are targets of clobetasol. (A) A representative experiment from two biological repeats, each with *n*=3, showing the relative expression of *CDKN1A*, *CDKN2A* and *CDKN2B* mRNAs determined by RT-qPCR, and normalized to the expression level in proliferation P, ethanol and DMSO, 24 h. D6, D12, D24, D48, doxycycline (1000 ng ml^{-1}) and DMSO for 6, 12, 24 or 48 h; DC24, DC48, doxycycline (1000 ng ml^{-1}) and clobetasol (2 nM) for 24 or 48 h. Error bars show s.d. (B) Representative western blot (*n*=3) of p15, p16 and p21 at various indicated times (hours) after doxycycline (1000 ng ml^{-1}) and DMSO or clobetasol (2 nM). A portion of the membrane with Revert protein stain is shown as a loading control (C) Number of cells after treatment with siRNAs for 24 h as indicated, then incubation with ethanol/DMSO (Prolif) or DMSO/doxycycline 1000 ng ml^{-1} (Dox) or doxycycline 1000 ng ml^{-1} and clobetasol 2 nM (DoxClob) for 96 h. A representative experiment from three biological repeats each with *n*=3 is shown. Error bars show s.d.

clobetasol, and EGR1 contributed to the expression of *CDKN1A* and *CDKN2B*.

Intriguingly, depletions of EGR1 or p15 and p21 with continuous clobetasol treatment allowed more proliferation than clobetasol treatment alone, and in the case of EGR1 and p15+p21 depletions, significantly more proliferation than for control cells that did not express B-RAF-V600E (Fig. 5C). The siRNA-mediated depletion of EGR1, p15 and p21 decreased the corresponding protein levels to a greater extent than clobetasol treatment (Figs. 4C, 5B and Fig. S7A,B). Thus, while clobetasol treatment alone, and depletions of EGR1, p21 or p15+p21 in the absence of clobetasol, allow cells to proliferate even when they express B-RAF-V600E, the combination of clobetasol and depletion of EGR1 and p15+p21 allows a 'hyper-proliferation'. This suggests that clobetasol has targets in addition to EGR, p15 and p21 that participate in the repression of proliferation driven by the hyper-activation of the B-RAF/MAPK pathway. Furthermore, whereas depletion of EGR1 and clobetasol treatment have similar effects in promoting proliferation after expression of B-RAF-V600E (Fig. 5C), the modest decrease of EGR1 protein levels in response to clobetasol is unlikely to explain all the effects of clobetasol. Hence, clobetasol would have other targets and/or clobetasol would interfere with EGR1 function at additional levels.

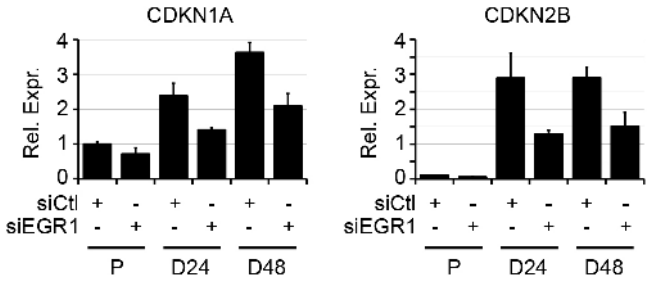

Fig. 6. EGR1 contributes to the transcriptional activation of *CDKN1A* and *CDKN2B*. Representative experiment showing the relative expression of *CDKN1A* and *CDKN2B* determined by RT-qPCR, and normalized to the expression level in proliferation (P, siCtl). Treatment with siRNAs (siCtl, siEGR1) for 24 h as indicated, then incubated with doxycycline 1000 ng ml^{-1} for 24 or 48 h (D24, D48) before harvest, or harvested after 24 h with ethanol (vehicle for doxycycline). Error bars show s.d. A representative experiment from two biological repeats each with *n*=3 is shown.

Depletion of EGR1 by transient siRNA knockdown greatly stimulated proliferation after B-RAF-V600E expression. We isolated two independent EGR1-KO (knockout) cell lines generated by CRISPR-Cas9-double nickase genome edition to test whether the KO of EGR1 would allow a permanent bypass of RAF-induced senescence. Upon expression of BRAF-V600E, the EGR1-KO cells proliferated longer than the WT cells (Fig. 8A; Fig. S7C), but eventually ceased proliferation (Fig. 8A). Hence, although EGR1 appears to be required for the rapid proliferative arrest after B-RAF-V600E expression, it is not required for senescence induction. In the EGR1-KO cells, clobetasol also allowed full senescence bypass when cells were regularly passaged (Fig. 8B), thus confirming the existence of other glucocorticoid targets. These results suggest that EGR1 acts as a transducer that controls the rapidity of the senescence proliferative arrest as a function of the hyper-activity of the ERK1/2 pathway.

DISCUSSION

Expression of hyper-mitogenic oncogenes, such as RASval12 and B-RAF-V600E, in normal human cells can trigger senescence in a process that is considered to act as a tumor suppressor mechanism (Collado and Serrano, 2010). DNA damage subsequent to replicative stress is implicated in the proliferative arrest associated with RASval12 expression (Di Micco et al., 2006), but does not appear to play an essential role in the senescence induced by hyperactive RAF kinases (Damsky and Bosenberg, 2017; Jeanblanc et al., 2012). Alternatively, signaling pathways may detect hyper-active ERK1/2 MAPK activity and trigger senescence. Indeed, in many developmental contexts, ERK1/2 activity governs cell fate decisions (Binétruy et al., 2007). Differentiation of PC12 pheochromocytoma cells is a well-studied example. Low-level transient activation of the ERK1/2 pathway by treating these cells with EGF is required for cellular proliferation whereas sustained high-level activation of the pathway mediated by NGF leads to a proliferative arrest and differentiation (Rauch et al., 2016). We found that glucocorticoids delayed or bypassed the senescence induced by expression of the B-RAF-V600E oncogene in human

Journal of Cell Science (2019) 132, jcs230748. doi:10.1242/jcs.230748

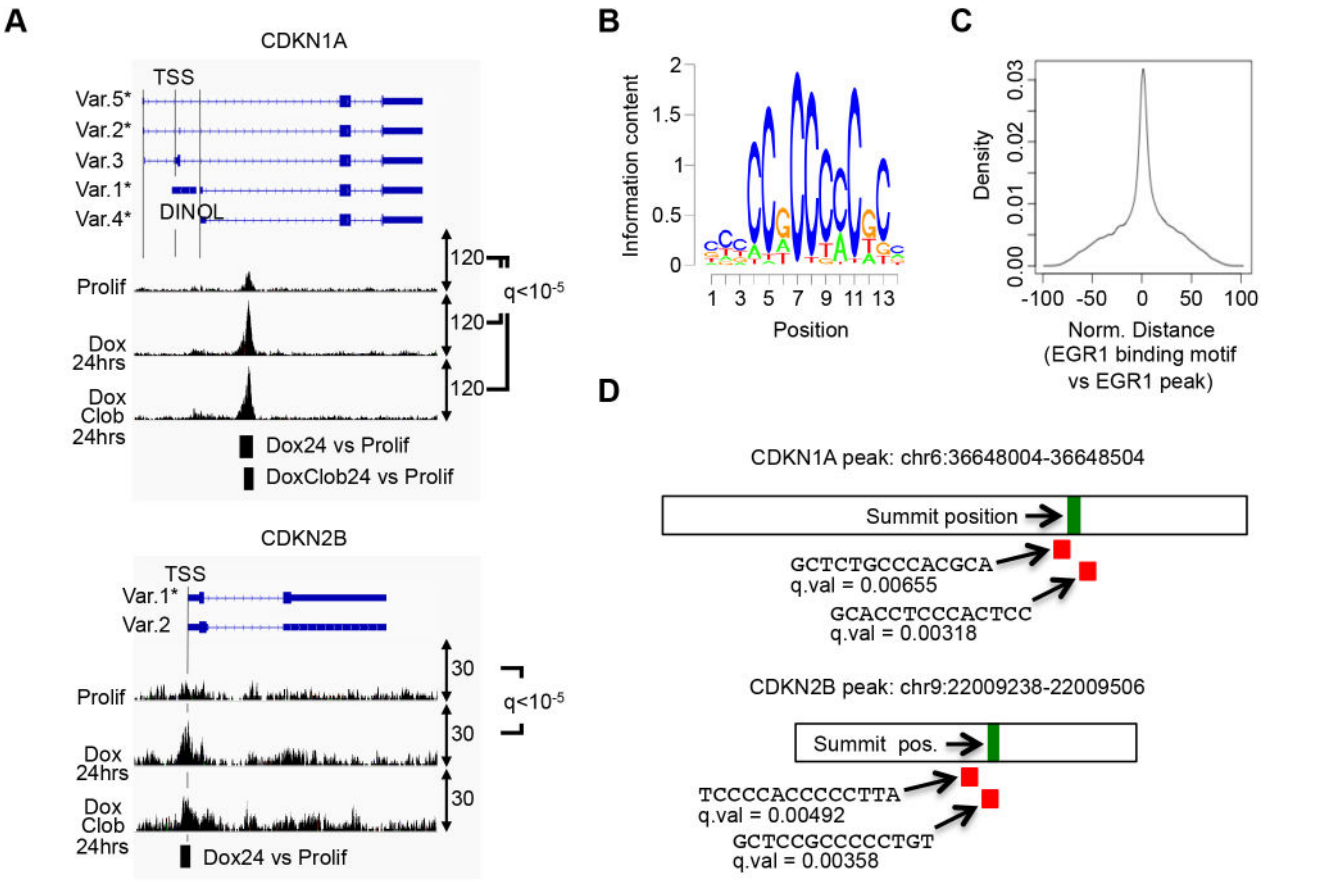

Fig. 7. EGR1 binds the *CDKN1A* and *CDKN2B* genes and EGR1-binding peaks encompass EGR1 binding motifs. (A) EGR1 binding to *CDKN1A* and *CDKN2B* genomic loci determined by paired-end ChIP-seq and peak-calling with MACS2 (q=FDR<1×10^{-5}) using 'Prolif' as background to identify differential peaks with 'Dox24hrs' or 'DoxClob24hrs'. Cells treated for 24 h with ethanol (vehicle for doxycycline) and DMSO (vehicle for clobetasol) (Prolif), doxycycline 1000 ng ml^{-1} and DMSO (Dox24hrs) or doxycycline 1000 ng ml^{-1} and clobetasol 2 nM (DoxClob24hrs). Numerical values, number of reads. (B) SeqLogo for motif 'MA0162.2' from JASPAR (http://jaspar.genereg.net/; Khan et al., 2018). MA0162.2 is derived from 12256 EGR1-binding sequences from ENCODE ChIPseq. (C) Kernel density plot of the distance normalized to the length of the peak, between the maximum of the peak and each EGR1 motif identified at FDR<0.01 by FIMO (Grant et al., 2011). (D) EGR1 peaks identified on *CDKN1A* and *CDKN2B* genes encompass EGR1-binding motifs close to the maximum of the peak. Box, representation of the peak corresponding to genomic coordinates as indicated; peak summit position and width as a green box. Red boxes, position of EGR1 consensus binding sites (and q-values associated with the sequence vs consensus calculated by FIMO).

fibroblasts, but did not revert the established senescent state. We used glucocorticoids as probes to dissect the signaling pathways involved in triggering RAF-induced senescence. Transcriptome analyses and siRNA knockdown experiments allowed us to identify the *EGR1* gene as one target of glucocorticoid action, but epistatic and phenotypic analyses indicated that glucocorticoids must also target other yet to be identified genes. E2F7 may be one such gene since its transcriptional activation by B-RAF-V600E is inhibited by clobetasol (Fig. 3C) and it was previously shown to contribute to senescence induced by RASval12 (Aksoy et al., 2012).

Expression of B-RAF-V600E leads to rapid activation of the MEK1/2 and ERK1/2 kinases (Fig. 2E) followed by transcriptional activation of the *EGR1* gene. ERK1/2 activates EGR1 transcription by phosphorylating the ELK1 subunit of the SRF transcription factor (Bahrami and Drabløs, 2016). EGR1 expression can thus act as a sensor of ERK1/2 MAPK activity triggering a rapid cell cycle arrest. EGR1 has been previously implicated in the replicative senescence of murine embryonic fibroblasts through transcriptional activation of the *TP53* gene (Krones-Herzig et al., 2003), and in a senescent-like cell cycle arrest associated with megakaryocyte maturation by activating *CDKN1A* transcription (Besancenot et al., 2010). In our model, EGR1 does not appear to activate *TP53* expression (data not shown and Fig. S5B), but the increased levels of EGR1 after B-RAF-V600E are associated with increased EGR1 genomic occupancy at the *CDKN2B* and *CDKN1A* genes and increased expression of these genes (Figs 6 and 7). In BJ fibroblasts, p15 and p21, but not p16, are required for the initial proliferative arrest induced by B-RAF-V600E expression (Fig. 5C). *CDKN2B* was recently shown to play an important role in RAF-induced senescence of melanocytes (McNeal et al., 2015). A role for *CDKN1A* in the RAF-induced senescence of melanocytes has not been directly demonstrated to our knowledge, although it was suggested that a dominant-negative TP53-R248W mutation facilitates melanomagenesis by decreasing *CDKN1A* expression (McNeal et al., 2015). Our work with BJ fibroblasts showed that EGR1 appears to trigger rapid senescence in response to B-RAF-V600E expression at least in part by binding to the *CDKN1A* and *CDKN2B* genes and increasing their expression. Although *CDKN2A* is a melanoma suppressor gene, it is not required for RAF-induced senescence (McNeal et al., 2015; Michaloglou et al., 2005). Individuals with *CDKN2A*-inactivating mutations tend to form larger and more numerous nevi, which suggests that p16 contributes to the proliferative arrest of melanocytes in response to B-RAF-V600E expression in a non-essential fashion in cooperation

Journal of Cell Science (2019) 132, jcs230748. doi:10.1242/jcs.230748

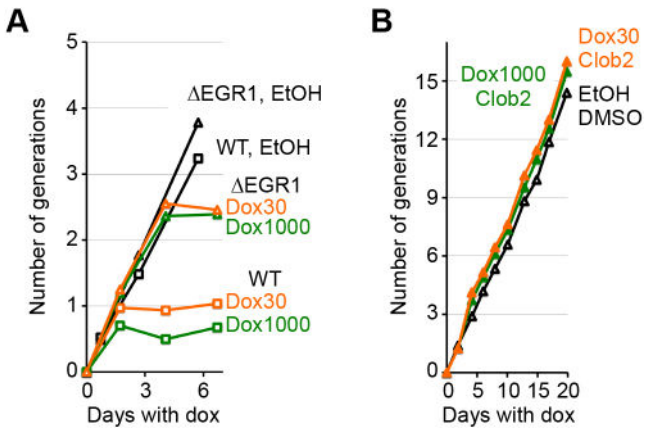

Fig. 8. The knockout of EGR1 delays, but does not bypass, RAF-induced senescence. (A,B) Number of cumulative generations. Cells were incubated with DMSO (vehicle for clobetasol) and drugs as indicated and counted every 2–3 days. Dox30, Dox1000, doxycycline 30 or 1000 ng ml^{-1}; EtOH, ethanol (vehicle for doxycycline); Clob2, clobetasol 2 nM. Representative experiments from two biological repeats each with n=3 are shown. In A, comparison of WT and ΔEGR1 cell lines in the absence of passaging. In B, ΔEGR1 cells were systematically passaged every 2–3 days, counted and re-seeded with the indicated drugs.

with other cell cycle inhibitors (Damsky and Bosenberg, 2017). Although p16 was not required for the initial proliferative arrest of BJ fibroblasts to B-RAF-V600E expression, it is possible that it contributes to longer maintenance of the senescent state or to the delayed proliferative arrest observed in the EGR1-KO cell line.

Glucocorticoid interference with senescence has the potential to increase cancer progression. Although no association between glucocorticoid usage and malignant melanoma was found in a population-based study (Jensen et al., 2009), there is one case report where treatment of a keloid lesion with a unique dose of the glucocorticoid triamcinolone, five years after melanoma removal, resulted in tumor recurrence (Lazarus and Kaufman, 2012). In addition, long-term use of medium- or high-dose systemic glucocorticoids slightly increased the risk of localized colorectal cancer, where 10% of tumors express mutated B-RAF (Ostenfeld et al., 2013). In skin cancers not related to B-RAF mutations, the risks of basal cell carcinoma and, to a lesser extent squamous cell carcinomas, were associated with glucocorticoid usage (Jensen et al., 2009). In both cases, senescence evasion may to be required for cancer progression, as has been reported for head and neck squamous cell carcinoma (Bian et al., 2012). Loss of heterozygosity of PTCH1, which is frequent in basal cell carcinoma and in SHH cerebellum medulloblastoma, has been shown to trigger senescence in preneoplastic medulloblastoma lesions (Tamayo-Orrego et al., 2016), and senescence features have been reported in basal cell carcinoma (Hida et al., 2009; Zhang et al., 2016). Hence, in addition to weakening immune surveillance of cancer, glucocorticoids could participate in senescence evasion. Three factors may mitigate this risk. First, glucocorticoids do not reverse the proliferative arrest of cells that were previously induced into senescence. Second, only in regularly passaged fibroblasts do glucocorticoids allow full bypass of senescence through mechanisms that remain to be identified. Third, gene regulation by the GR is highly cell-type specific. It will be important in the future to evaluate the effect of glucocorticoid treatment on RAF-induced senescence of melanocytes and thyroid and colonic epithelial cells that are the principal cell types subject to tumorigenesis driven by B-RAF-V600E, and more generally on cell types where senescence is a feature in preneoplasia. In any event, further analysis of glucocorticoid action should reveal additional genes that contribute to RAF-induced senescence.

MATERIALS AND METHODS

Materials

The drug repositioning chemical library was purchased from Prestwick Chemical (Illkirch, France). Clobetasol propionate, cortisol, and RU-486 (mifepristone) were purchased from Sigma-Aldrich. Compound A was purchased from Enzo Life Sciences.

Cell lines and cell culture

The BJ1-hTert (BJhTert) cell line was purchased from Clontech and stably infected with pTRIPZ-3HA-B-RAF-V600E. A synthetic gene encoding the B-RAF-V600E coding sequence with a 3-HA N-terminal tag was inserted as an AgeI-MluI fragment into the AgeI-MluI digested lentiviral pTRIPz vector (Thermo Fisher Scientific). This cloning placed the 3HA-B-RAF-V600E coding sequence under the control of the pTRIPz ptet-ON promoter. The pBabe-puro-IkB-SR plasmid was a generous gift of Denis Guttridge (Ohio State University Medical Center, USA) (Wang et al., 2009). Retrovirus/lentivirus were prepared by $CaCl_2$ co-transfection of 293T cells with viral plasmids and the appropriate packaging plasmids as described previously (Barde et al., 2010). The BJ1-hTert cells were infected with pTRIPz-3HA-B-RAF-V600E lentivirus and a population of infected cells was selected for 1 µg ml^{-1} puromycin resistance. BJ1-hTert/pTRIPz-3HA-B-RAF-V600E cells were subsequently super-infected with pBabe-puro-IkB-SR virus until more than 85% of cells showed an absence of RelA nuclear translocation after treating cells with 10 ng ml^{-1} TNF for 30 min. The WI38hTert cell line and derivatives were described previously (Jeanblanc et al., 2012). IMR90/ER-RasV12 (for expression of RASval12) cells were a kind gift of Masashi Narita (Cambridge Research Institute, CRUK, Cambridge, UK) (Young et al., 2009). They were nucleofected with linearized pBabe-hygro-hTert (Jeanblanc et al., 2012), then hygromycin B-resistant clones were trypsinized and amplified together to give an immortal cell population. Senescence was induced with doxycycline (D3447, Sigma-Aldrich) for the expression of B-RAF-V600E and with 4-hydroxy-tamoxifen (H6278, Sigma-Aldrich) for the expression of C-RAF and RASval12. Cells were grown in MEM (Gibco #51200, Thermo Fisher Scientific) with 10% fetal bovine serum, 2 mM Glutamax (A12860, Gibco), 1× MEM non-essential amino acids (M7145, Sigma-Aldrich) and 1 mM sodium pyruvate (S8636, Sigma-Aldrich). WI38hTert and IMR90hTert cells were cultured in a 5% carbon dioxide and 5% oxygen incubator whereas BJhTert cells were cultured in 5% carbon dioxide and ambient oxygen. Cells were mycoplasma negative.

siRNA knockdown

Cells were seeded in CostarAssay 96-well plates (Ref 3904, Corning, SigmaAldrich) and 24 h later transfected with Lipofectamine RNAiMax (Invitrogen, Thermo Fisher Scientific) following the manufacturer's instructions. When indicated, cells were treated with drugs 24 h after transfection. siRNA experiments were generally carried out in triplicates in 96-well plates. See Table S4 for the list of siRNAs.

EGR1 knockout

BJhTert cells line stably infected with pTRIPZ-3HA-BRAF-V600E were transiently transfected with pAIO-GFP-EGR1 to knockout EGR1 in a double-nickase approach (Chiang et al., 2016). The sgRNA sequences targeting the end of EGR1 exon 1 (sense: 5′-CCCTACGAGCACCTGAC-CGC-3′; antisense: 5′-CGTGTCCGCCTGAGGGTTGAAGG-3′) were subcloned in pAIO-GFP (Addgene 74119). GFP fluorescent cells were sorted in batch and seeded in a 96-well plate (limit dilution) with etoposide-induced senescent BJhTert as feeder cells to support the proliferation of the transfected fibroblasts plated at limiting dilutions. After 10 days in culture, feeder cells were eliminated, and pAIO-GFP transiently transfected cells were selected with puromycin. After amplification of individual clones, the plate was duplicated and EGR1-negative clones were screened by immunofluorescence using Cell Signaling Technologies CST4154 antibody. EGR1-negative clones were sequenced to determine indel events. For clone C7 used in this study, indel sequences were

CA*ACCCTCAGGCGGACAC---------agggctg--------GAC*C and CA*ACCCTCAGGCG----------ag----------TGAC*C (uppercase: wild-type sequence, *: single-strand break site). For clone A9 only one indel sequence was obtained: CA*ACCCTCAGGCGGACACG----------t----------AGG.

High-content microscopy

Cell counting

Cells grown in CostarAssay 96-well plates (Ref 3904, Corning, Sigma-Aldrich) were fixed with 1.6% paraformaldehyde (Sigma-Aldrich) and stained with and bisbenzimide trihydrochloride (Hoechst 33342, Sigma-Aldrich) at 50 µg ml^{-1} (final concentrations). Following automatic segmentation, the nuclei were counted on a high-content screening microscope [Operetta from Perkin-Elmer (Courtaboeuf, FR) or CellInsight CX5 from Thermo Fisher Scientific].

Measure of DNA replication

Cell ability to replicate DNA over 48-h windows was determined by the incorporation of the nucleotide analogue 5-ethynyl-2′-deoxyuridine (EdU) in neo-synthesized DNA. EdU was subsequently revealed by click-chemistry using Click-iT EdU AlexaFluor imaging kits (Thermo Fisher Scientific) following the manufacturer's instructions. Nuclei were also stained with 50 µg ml^{-1} Hoechst 33342. Nuclei staining was used for automatic segmentation and determination of EdU-positive nuclei on a high-content screening microscope (Operetta from Perkin-Elmer or CellInsight CX5 from Thermo Fisher Scientific).

SAHF formation

Cells were fixed as described above and nuclei were stained with 4′,6-diamidino-2-phénylindole (DAPI, 0.5 µg ml^{-1}). Following imaging on the CellInsight CX5 high-content screening microscope (Thermo Fisher Scientific), nuclei were automatically segmented and the mean and standard deviation of nuclear DAPI intensity were determined for all nuclei and used to calculate the DAPI CV (s.d. as a percentage of the mean) as previously described (Contrepois et al., 2012).

Immunofluorescence

Cells were fixed as described above and stained with anti-EGR1 antibody (CST4154, lot 3, 1:1000) with permeabilization, washes, and secondary 488 nm antibodies as described (Jeanblanc et al., 2012). Following imaging on the CellInsight CX5 high-content screening microscope (Thermo Fisher Scientific), nuclei were automatically segmented and the integrated intensity for EGR1 staining recovered for each nucleus for processing in R (script available upon request).

Screening of the Prestwick chemical library

WI-38hTert/C-RAF-ER cells where senescence was induced with 20 nM 4-hydroxytamoxifen (Jeanblanc et al., 2012) were incubated with 1030 molecules from the Prestwick drug repositioning library. The final concentration of the drugs was 35 µM in 0.35% DMSO. Cells were incubated with the drugs for 4 days before the number of cells was evaluated as described above (Cell counting). The primary screen was carried out in duplicate plates. For each plate, the mean number of cells and the corresponding standard deviation were calculated in eight negative control wells (DMSO only). From this, we calculated the coefficient of variation for the negative control (CV, s.d. as a percentage of the mean), and the plate was considered valid only if the CV was less than 5%. For every well, we calculated a score corresponding to the number of cells in the well minus the mean number of cells of the negative controls, divided by the standard deviation of the negative controls. For each molecule, we thus had two *z*-scores, corresponding to the difference in number of cells with the molecule assayed and with the negative control, expressed as the number of standard deviations of the negative control. A molecule was determined a hit if its score was higher than five in both replicates. Of the 1030 molecules assayed, 40 (4%) were positive, including all the glucocorticoids of the Prestwick library: fluticasone proprionate (scores: 40,29), triamcinolone (33,32), alclometasone diproprionate (35,25), fluocinonide (25,23), clocortolone pivalate (20,32), mometasone furoate (21,41), betamethasone (19,20), rimexolone (23,20), diflorasone diacetate (19,34), beclomethasone dipropionate (26,39), fluorometholone (39,26), dexamethasone acetate (23,25), flumethasone (23,20), flunisolide (24,33), clobetasol proprionate (19,17), halcinonide (30,22), flurandrenolide (20,27), hydrocortisone base (15,22), budesonide (12,26), fludrocortisone acetate (26,28), 6-alpha methylprednisolone (25,25), prednisolone (24,23), medrysone (13,11), corticosterone (8,10), prednicarbate (5,6), and cortisone (10,11). Other hits had scores ranging from (5,6) to (22,46). We used clobetasol proprionate for further experiments to characterize the mechanism of glucocorticoid action in suppressing RAF-induced senescence.

SA-β-galactosidase staining

SA-β-gal assays were performed by staining formaldehyde (3%)-fixed cells with 1 mg ml^{-1} 5-bromo-4-chloro-3-indolyl-β-D-galactoside (X-Gal) in 40 mM citric acid-sodium phosphate (pH 6.0), 5 mM potassium ferrocyanide/5 mM potassium ferricyanide, 150 mM NaCl and 2 mM $MgCl_2$ buffer overnight at 37°C. Images were acquired on an Olympus SZ61 stereomicroscope at 2.5× magnification with a Moticam 2300 camera (MoticEurope, Barcelona, Spain).

Growth curves

Cells were grown in 10-cm dishes with the indicated drugs. Cells were trypsinised every 2–3 days, unless unnecessary, using trypsin-EDTA (1 g/l porcine trypsin, 0.4 g/l EDTA in PBS, 2′ incubation). Cells in suspension were counted using an automated cell counter (Scepter, MerkMillipore, Saint-Quentin-en-Yvelines, FR) and 60 µm sensors (#PHCC60050) within the linear range of the apparatus. Cells were seeded at a density of 300,000 per 10-cm dish.

SDS-PAGE and western blotting

Whole-cell extracts were harvested by scraping cells in PBS at room temperature, centrifugation at 500 ***g*** and resuspension/lysis in 1× SDS-PAGE sample buffer with protease inhibitors (Complete EDTA-free #11836170001, Roche, Sigma-Aldrich) and phosphatase inhibitor cocktail (B15001-A&B, Biotools, Euromedex, Souffelweyersheim, France). Extracts were incubated at 70°C for 10 min before freezing. After thawing, the extracts were briefly sonicated to reduce viscosity. Samples were first normalized on a Bis-Tris-MOPS SDS-PAGE with in-gel staining with Instant Blue and quantification on a LiCor NIR scanner (Odyssey Classic or CLx, 700 nm channel, LI-COR Biosciences GmbH, Bad Homburg, Germany). When necessary, sample concentrations were matched using 1× sample buffer as diluent.

After 11% SDS-PAGE, proteins were transferred to nitrocellulose membranes (Protran 0.2 µm, #10600001, GE Healthcare). Membranes were blocked with LiCor Odyssey Blocking Buffer (PBS) (#927-4000), diluted 1:1 in PBS and incubated with primary antibody overnight at 4°C. NIR-secondary antibodies were revealed using the Li-Cor Odyssey infrared imaging system following the manufacturer's protocols. Antibodies were from Santa Cruz Biotechnologies [anti-B-RAF sc5284, lot I3013, 1:1000 (Fig. 1B), sc-166, lot G2408, 1:1000 (Fig. 2C), anti-EGR1 sc-189X, lot B2315, 1:10000 (Fig. 4C), anti-p15 sc-612, lot E9008, 1:1000 (Fig. 5B)], Cell Signaling Technologies [anti-phospho-MEK1/2, CST9121, lot 47, 1:1000 (Fig. 2C), anti-phospho-ERK1/2, CST9106, lot 45, 1:1000 (Fig. 2C), anti-ERK1/2, CST4695, lot 5, 1:1000 (Fig. 2C), anti-p21, CST2947, lot 10, 1:1000 (Fig. 5B)] and BD Pharmingen [anti-p16, 554079, lot 5044728, 1:250). Unless otherwise indicated, membranes were stained with the Revert stain (LiCor) which was used for quantification and normalization after imaging on the LiCor Odyssey at 700 nm. Alternatively, 2,2,2-trichloroethanol (TCE) staining of tryptophan residues was used for normalization after UV irradiation (Ladner et al., 2004).

To quantify the level of doxycycline-inducible B-RAF-V600E relative to endogenous B-RAF, we added a 3HA epitope tag to the N-terminus of the B-RAF-V600E protein (see description of cell lines above) so that we could distinguish it from the endogenous WT B-RAF protein by its slightly slower migration on SDS-PAGE gels. This allowed us to estimate the relative expression of B-RAF-V600E to endogenous B-RAF by quantifying the relative intensity of the two bands in anti-B-RAF western blots visualized with the LiCor Odyssey scanner.

RNA extraction

BJhTert-BRAF-V600E cells were grown in the presence of doxycycline (or ethanol as control) and clobetasol (or DMSO as control) for the indicated durations and at the indicated concentrations. RNA was extracted using the NucleoSpin RNA kits (Macherey Nagel, Hoerdt, FR) following the manufacturer's instructions.

RT-qPCR

The total RNA yield was determined spectrophotometrically with a Nanodrop 2000 (Thermo Fisher Scientific) and reverse transcription was carried out with random hexamer primers from 500 or 1000 ng RNA with the Maxima Reverse Transcriptase (Thermo Fisher Scientific). cDNA was diluted 1:10 for quantitative (q)PCR which was performed with a Luminaris Color HiGreen qPCR Master Mix (Thermo Fisher Scientific) and monitored on an IQ5 apparatus (Bio-Rad) following the manufacturer's instructions. GAPDH was used for normalization. See Table S3 for the list of primers.

Illumina bead chip array transcriptome analyses

BJhTert-BRAF-V600E cells were grown with drugs as indicated, and triplicates were harvested as described above. The total RNA yield was determined spectrophotometrically using the NanoDrop ND-100 (Labtech, Palaiseau, France). Total RNA profiles were recorded using a Bioanalyzer 2100 (Agilent). RNA integrity numbers were determined, and the mean value found was 9.94±0.14 (±s.d.). The coefficient of variation (CV) was 1.32%. cRNA was synthesized, amplified and purified with the TargetAmp™ Nano Labeling Kit for Illumina® Expression BeadChip® (Epicentre, Illumina, Evry, France) following the manufacturer's instructions. Briefly, 100 ng of RNA were reverse transcribed. After second strand synthesis, the cDNA was transcribed *in vitro* and cRNA labeled with biotin-UTP. Labeled probes were then hybridized with beads using Illumina Bead Chip human HT-12 v4 arrays. These bead chips contain 47,231 unique 50-mer oligonucleotides in total, with hybridization to each probe assessed at 15 different beads on average. 28,403 probes (60.7%) are targeted at Reference Sequence (RefSeq) transcripts and the remaining 18,543 (39.3%) are for other transcripts, generally less well characterized (including predicted transcripts).

Bead Chips were scanned on the Illumina iScan Reader using Illumina iScan control software version 3 and Illumina Genome Studio software (version 2011.1) were used for preliminary data analysis. Multiple quality controls were performed and analyzed with the Illumina Genome Studio software, including scatter plots of control RNA samples from different labeling runs. The scatter plots compared duplicated control and experimental samples and were used to calculate correlation coefficients. These comparisons determined whether controls and samples from different labeling runs varied in quality. The control summary report generated by Genome Studio evaluates variations in signal intensity, hybridization signal, background signal, and the background/noise ratio for all the samples analyzed in that run. The Illumina idat files have been deposited in the GEO database under accession number GSE134747.

Bead chip bioinformatics analysis

Raw bead chip array intensity data contained in the proprietary Illumina .idat files were analyzed using open-source Bioconductor packages. Data was retrieved from the .idat files using the bead array package (Dunning et al., 2007). Data were quantile normalized with control probes using the neqc function in the limma R package (Ritchie et al., 2015). Batch effects were corrected with the sva package (Leek et al., 2012). The gene symbols corresponding to Illumina probe ids were retrieved with the Illumina HumanHT12v4 annotation data. Differential gene expression analysis was performed with the limma package and heat maps were constructed with pheatmap. R scripts used for the transcriptomic analyses are available upon request.

EGR1 ChIP-seq and peak-calling

10 million cells were used for each ChIP (5 million fibroblasts/15 cm dish). Cells were fixed in 1% final concentration of EM-grade formaldehyde for 10 min and then quenched by the addition of glycine to a final concentration of 0.2 M for 10 min. Cells were washed once with cold PBS and then scraped in cold PBS, centrifuged, and washed again with cold PBS. Cells were then resuspended in 1 ml of cold IP buffer (10 mM Tris-HCl pH 8, 100 mM NaCl, 1 mM EDTA, 0.5 mM EGTA, 0.1% sodium deoxycholate, 0.5% N-lauroylsarcosine sodium salt) and sonicated in a Covaris S220 machine (Brighton, UK) with the following parameters: 150 W, 10%, 200 bursts/cycle, 5×2 min. Then 20 µl was removed after sonication to verify the correct size of the sonicated DNA. After verification, 250 µl of sonicated chromatin was diluted with 500 µl of cold IP buffer containing additionally Roche protease inhibitor cocktail. 12.5 µl (5%) was removed to isolate input DNA. 6 µg of anti-EGR1 antibody (sc-189X) was then added for each IP and incubated overnight with rotation at 4°C. 30 µl of protein G–Sepharose beads that had been blocked by incubation with LB3-containing 2% BSA were then added to the IP solution and incubated for 2 h with rotation at 4°C. The beads were then washed once consecutively with WB1 (20 mM Tris-HCl pH 8, 150 mM NaCl, 2 mM EDTA, 0.1% SDS, 0.25% Triton-X-100), WB1 with 500 mM NaCl, WB2 (10 mM Tris-HCl pH 8, 250 mM LiCl, 1 mM EDTA, 0.1% sodium deoxycholate, 1% Igepal CA-630), and TE (10 mM Tris-HCl pH 8, 1 mM EDTA). The washed beads were then resuspended in 200 µl of TE+1% SDS. 1 µl (20 µg) of proteinase K solution was added and the suspension was incubated with shaking overnight at 65°C in a Thermomixer (Eppendorf, Dutscher) to digest proteins and to reverse the formaldehyde crosslinks. Immunoprecipitated DNA was then purified by phenol/chloroform extraction and ethanol precipitation. A DNA library for sequencing was prepared with a Diagenode IP-Star platform (Diagenode, Seraing, Belgium) using their MicroPlex Library Preparation kit v2. Amplified DNA fragments with ligated sequence adapters were sized to ∼325 bp with AMPure XP beads (A63880, Beckman Coulter). The size of the final library fragments was verified on an Agilent Bioanalyzer and DNA concentrations were determined with an Invitrogen Qubit fluorimeter. Sequencing was performed by the NGS platform at the I2BC. Libraries were pooled in equimolar proportions and sequenced on an Illumina NextSeq500 instrument, using NextSeq 500/550 High Output 75 cycles kits; 43 (Paired end) sequencing cycles were performed. Demultiplexing was undertaken with bcl2fastq2 V2-2.18.12, adapters removed with Cutadapt v1.15, and reads longer than 10 pb were kept for analysis. FastQC v0.11.5 was used for quality control. The final number of reads was between 28 and 68 million for each sample. Three replicates were sequenced per condition. Reads were mapped to the human genome (hg19) using bwa-sampe (0.7.15-r1140), and samtools (1.3.1, using htslib 1.3.2) was used to sort, index and remove duplicates. FastQ files have been deposited in the GEO database under accession number GSE134924.

Peak-calling was performed using MACS2 (2.1.1.20160309, https://github.com/taoliu/MACS) using the BAMPE option, collecting all peaks irrespective of the reported q-value. Peaks with q-value lower than 1×10^{-5} were selected with R. Peaks were differentially called using three replicates for each condition (24 h treatment): doxycycline+DMSO vs ethanol+DMSO and doxycycline+clobetasol vs ethanol+DMSO. The specificity of the peaks was estimated in two ways. First, 73% of the peaks called by MACS2 were found to overlap peaks for EGR1 already identified by ENCODE (48341 peaks concatenated from data from K562, hESC, ECC, HCT116 and MCF7 cells). Second, FIMO (meme-suite.org/tools/fimo) was used to identify occurrences of the EGR1-binding motif (Fig. 7B) in peaks identified in this study. At a FDR<0.01, 80% of the peaks identified by MACS2 (doxycycline+DMSO vs ethanol+DMSO) had at least one EGR1-binding motif. Furthermore, the EGR1-binding motif was highly correlated with the maximum of the peak (Fig. 7C). 81% of the peaks identified by MACS2 that had at least one EGR1-binding motif had already been identified by ENCODE.

Acknowledgements

We thank Cécile Dulary et Virginie Lavilla for their technical help. This work has benefited from the platform and expertise of the High-throughput Sequencing Platform of the I2BC.

Competing interests

The authors declare no competing or financial interests.

Author contributions

Conceptualization: C.M., J.-Y.T.; Validation: G.P., R.O., C.M., J.-Y.T.; Formal analysis: G.K., J.-Y.T.; Investigation: C.C., V.L., R.C., G.K., C.Derbois, J.-Y.T.;

Resources: G.P., J.-C.C., C.Denby-Wilkes, R.O., J.-F.D.; Data curation: J.-Y.T.; Writing - original draft: C.M., J.-Y.T.; Writing - review & editing: C.C., V.L., C.M., J.-Y.T.; Visualization: J.-Y.T.; Supervision: C.M., J.-Y.T.; Project administration: C.M., J.-Y.T.; Funding acquisition: C.M., J.-Y.T.

Funding

This work was supported with funding by the Fondation ARC pour la Recherche sur le Cancer, Fondation pour la Recherche Médicale, the GEFLUC Paris Ile-De-France, and the Ligue Contre le Cancer (Comité Val d'Oise).

Data availability

Illumina bead chip array transcriptome analyses and ChIP-seq results have been deposited, in the GEO database under accession numbers GSE134747 and GSE134924, respectively.

Supplementary information

Supplementary information available online at
http://jcs.biologists.org/lookup/doi/10.1242/jcs.230748.supplemental

References

Aksoy, O., Chicas, A., Zeng, T., Zhao, Z., McCurrach, M., Wang, X. and Lowe, S. W. (2012). The atypical E2F family member E2F7 couples the p53 and RB pathways during cellular senescence. *Genes Dev.* **26**, 1546-1557. doi:10.1101/gad.196238.112

Bahrami, S. and Drabløs, F. (2016). Gene regulation in the immediate-early response process. *Adv. Biol. Regul.* **62**, 37-49. doi:10.1016/j.jbior.2016.05.001

Barde, I., Salmon, P. and Trono, D. (2010). Production and titration of lentiviral vectors. *Curr. Protoc. Neurosci.* **53**, 4.21.1-4.21.23. doi:10.1002/0471142301.ns0421s53

Beausejour, C. M., Krtolica, A., Galimi, F., Narita, M., Lowe, S. W., Yaswen, P. and Campisi, J. (2003). Reversal of human cellular senescence: roles of the p53 and p16 pathways. *EMBO J.* **22**, 4212-4222. doi:10.1093/emboj/cdg417

Besancenot, R., Chaligné, R., Tonetti, C., Pasquier, F., Marty, C., Lécluse, Y., Vainchenker, W., Constantinescu, S. N. and Giraudier, S. (2010). A senescence-like cell-cycle arrest occurs during megakaryocytic maturation: Implications for physiological and pathological megakaryocytic proliferation. *PLoS Biol.* **8**, e1000476. doi:10.1371/journal.pbio.1000476

Bian, Y., Hall, B., Sun, Z.-J., Molinolo, A., Chen, W., Gutkind, J. S., Waes, C. V. and Kulkarni, A. B. (2012). Loss of TGF-β signaling and PTEN promotes head and neck squamous cell carcinoma through cellular senescence evasion and cancer-related inflammation. *Oncogene* **31**, 3322-3332. doi:10.1038/onc.2011.494

Binétruy, B., Heasley, L., Bost, F., Caron, L. and Aouadi, M. (2007). Concise review: regulation of embryonic stem cell lineage commitment by mitogen-activated protein kinases. *Stem Cells* **25**, 1090-1095. doi:10.1634/stemcells.2006-0612

Cadepond, F., Ulmann, A. and Baulieu, E.-E. (1997). RU486 (MIFEPRISTONE): mechanisms of action and clinical uses. *Annu. Rev. Med.* **48**, 129-156. doi:10.1146/annurev.med.48.1.129

Cantwell-Dorris, E. R., O'Leary, J. J. and Sheils, O. M. (2011). BRAFV600E: implications for carcinogenesis and molecular therapy. *Mol. Cancer Ther.* **10**, 385-394. doi:10.1158/1535-7163.MCT-10-0799

Chiang, T.-W. W., le Sage, C., Larrieu, D., Demir, M. and Jackson, S. P. (2016). CRISPR-Cas9D10A nickase-based genotypic and phenotypic screening to enhance genome editing. *Sci. Rep.* **6**, 24356. doi:10.1038/srep24356

Chien, Y., Scuoppo, C., Wang, X., Fang, X., Balgley, B., Bolden, J. E., Premsrirut, P., Luo, W., Chicas, A., Lee, C. S. et al. (2011). Control of the senescence-associated secretory phenotype by NF-κB promotes senescence and enhances chemosensitivity. *Genes Dev.* **25**, 2125-2136. doi:10.1101/gad.17276711

Collado, M. and Serrano, M. (2010). Senescence in tumours: evidence from mice and humans. *Nat. Rev. Cancer* **10**, 51-57. doi:10.1038/nrc2772

Contrepois, K., Thuret, J.-Y., Courbeyrette, R., Fenaille, F. and Mann, C. (2012). Deacetylation of H4-K16Ac and heterochromatin assembly in senescence. *Epigenet. Chromatin* **5**, 15. doi:10.1186/1756-8935-5-15

Damsky, W. E. and Bosenberg, M. (2017). Melanocytic nevi and melanoma: unraveling a complex relationship. *Oncogene* **36**, 5771-5792. doi:10.1038/onc.2017.189

Di Micco, R., Fumagalli, M., Cicalese, A., Piccinin, S., Gasparini, P., Luise, C., Schurra, C., Garre', M., Nuciforo, P. G., Bensimon, A. et al. (2006). Oncogene-induced senescence is a DNA damage response triggered by DNA hyper-replication. *Nature* **444**, 638-642. doi:10.1038/nature05327

Dunning, M. J., Smith, M. L., Ritchie, M. E. and Tavare, S. (2007). beadarray: R classes and methods for Illumina bead-based data. *Bioinformatics* **23**, 2183-2184. doi:10.1093/bioinformatics/btm311

Fey, D., Matallanas, D., Rauch, J., Rukhlenko, O. S. and Kholodenko, B. N. (2016). The complexities and versatility of the RAS-to-ERK signalling system in normal and cancer cells. *Semin. Cell Dev. Biol.* **58**, 96-107. doi:10.1016/j.semcdb.2016.06.011

Grant, C. E., Bailey, T. L. and Noble, W. S. (2011). FIMO: scanning for occurrences of a given motif. *Bioinformatics* **27**, 1017-1018. doi:10.1093/bioinformatics/btr064

Hida, Y., Kubo, Y. and Arase, S. (2009). Activation of fibroblast growth factor receptor 3 and oncogene-induced senescence in skin tumours. *Br. J. Dermatol.* **160**, 1258-1263. doi:10.1111/j.1365-2133.2009.09068.x

Jeanblanc, M., Ragu, S., Gey, C., Contrepois, K., Courbeyrette, R., Thuret, J.-Y. and Mann, C. (2012). Parallel pathways in RAF-induced senescence and conditions for its reversion. *Oncogene* **31**, 3072-3085. doi:10.1038/onc.2011.481

Jensen, A., Thomsen, H. F., Engebjerg, M. C., Olesen, A. B., Friis, S., Karagas, M. R. and Sørensen, H. T. (2009). Use of oral glucocorticoids and risk of skin cancer and non-Hodgkin's lymphoma: a population-based case–control study. *Br. J. Cancer* **100**, 200-205. doi:10.1038/sj.bjc.6604796

Karin, M. and Ben-Neriah, Y. (2000). Phosphorylation meets ubiquitination: the control of NF-κB activity. *Annu. Rev. Immunol.* **18**, 621-663. doi:10.1146/annurev.immunol.18.1.621

Khan, A., Fornes, O., Stigliani, A., Gheorghe, M., Castro-Mondragon, J. A., van der Lee, R., Bessy, A., Chèneby, J., Kulkarni, S. R., Tan, G. et al. (2018). JASPAR 2018: update of the open-access database of transcription factor binding profiles and its web framework. *Nucleic Acids Res.* **46**, D260-D266. doi:10.1093/nar/gkx1126

Krones-Herzig, A., Adamson, E. and Mercola, D. (2003). Early growth response 1 protein, an upstream gatekeeper of the p53 tumor suppressor, controls replicative senescence. *Proc. Natl. Acad. Sci. USA* **100**, 3233-3238. doi:10.1073/pnas.2628034100

Laberge, R.-M., Zhou, L., Sarantos, M. R., Rodier, F., Freund, A., de Keizer, P. L. J., Liu, S., Demaria, M., Cong, Y.-S., Kapahi, P. et al. (2012). Glucocorticoids suppress selected components of the senescence-associated secretory phenotype. *Aging Cell* **11**, 569-578. doi:10.1111/j.1474-9726.2012.00818.x

Ladner, C. L., Yang, J., Turner, R. J. and Edwards, R. A. (2004). Visible fluorescent detection of proteins in polyacrylamide gels without staining. *Anal. Biochem.* **326**, 13-20. doi:10.1016/j.ab.2003.10.047

Lazarus, M. and Kaufman, H. (2012). An association between corticosteroid use and melanoma recurrence: a case report and review of the literature. *Med. Oncol.* **29**, 2018-2020. doi:10.1007/s12032-011-0064-0

Leek, J. T., Johnson, W. E., Parker, H. S., Jaffe, A. E. and Storey, J. D. (2012). The sva package for removing batch effects and other unwanted variation in high-throughput experiments. *Bioinformatics* **28**, 882-883. doi:10.1093/bioinformatics/bts034

Lesovaya, E., Yemelyanov, A., Swart, A. C., Swart, P., Haegeman, G. and Budunova, I. (2015). Discovery of compound A - a selective activator of the glucocorticoid receptor with anti-inflammatory and anti-cancer activity. *Oncotarget* **6**, 30730-30744. doi:10.18632/oncotarget.5078

Mawal-Dewan, M., Frisoni, L., Cristofalo, V. J. and Sell, C. (2003). Extension of replicative lifespan in WI-38 human fibroblasts by dexamethasone treatment is accompanied by suppression of p21Waf1/Cip1/Sdi1 levels. *Exp. Cell Res.* **285**, 91-98. doi:10.1016/S0014-4827(03)00013-2

McNeal, A. S., Liu, K., Nakhate, V., Natale, C. A., Duperret, E. K., Capell, B. C., Dentchev, T., Berger, S. L., Herlyn, M., Seykora, J. T. et al. (2015). CDKN2B loss promotes progression from benign melanocytic nevus to melanoma. *Cancer Discov.* **5**, 1072-1085. doi:10.1158/2159-8290.CD-15-0196

Michaloglou, C., Vredeveld, L. C. W., Soengas, M. S., Denoyelle, C., Kuilman, T., van der Horst, C. M. A. M., Majoor, D. M., Shay, J. W., Mooi, W. J. and Peeper, D. S. (2005). BRAFE600-associated senescence-like cell cycle arrest of human naevi. *Nature* **436**, 720-724. doi:10.1038/nature03890

Ostenfeld, E. B., Erichsen, R., Thorlacius-Ussing, O., Riis, A. H. and Sørensen, H. T. (2013). Use of systemic glucocorticoids and the risk of colorectal cancer. *Aliment. Pharmacol. Ther.* **37**, 146-152. doi:10.1111/apt.12115

Rauch, N., Rukhlenko, O. S., Kolch, W. and Kholodenko, B. N. (2016). MAPK kinase signalling dynamics regulate cell fate decisions and drug resistance. *Curr. Opin. Struct. Biol.* **41**, 151-158. doi:10.1016/j.sbi.2016.07.019

Ritchie, M. E., Phipson, B., Wu, D., Hu, Y., Law, C. W., Shi, W. and Smyth, G. K. (2015). limma powers differential expression analyses for RNA-sequencing and microarray studies. *Nucleic Acids Res.* **43**, e47-e47. doi:10.1093/nar/gkv007

Sacta, M. A., Chinenov, Y. and Rogatsky, I. (2016). Glucocorticoid signaling: an update from a genomic perspective. *Annu. Rev. Physiol.* **78**, 155-180. doi:10.1146/annurev-physiol-021115-105323

Salotti, J., Sakchaisri, K., Tourtellotte, W. G. and Johnson, P. F. (2015). An Arf-Egr-C/EBPβ pathway linked to Ras-induced senescence and cancer. *Mol. Cell. Biol.* **35**, 866-883. doi:10.1128/MCB.01489-14

Shain, A. H., Yeh, I., Kovalyshyn, I., Sriharan, A., Talevich, E., Gagnon, A., Dummer, R., North, J., Pincus, L., Ruben, B. et al. (2015). The genetic evolution of melanoma from precursor lesions. *N. Engl. J. Med.* **373**, 1926-1936. doi:10.1056/NEJMoa1502583

Tamayo-Orrego, L., Wu, C.-L., Bouchard, N., Khedher, A., Swikert, S. M., Remke, M., Skowron, P., Taylor, M. D. and Charron, F. (2016). Evasion of cell senescence leads to medulloblastoma progression. *Cell Rep.* **14**, 2925-2937. doi:10.1016/j.celrep.2016.02.061

Wang, J., Jacob, N. K., Ladner, K. J., Beg, A., Perko, J. D., Tanner, S. M., Liyanarachchi, S., Fishel, R. and Guttridge, D. C. (2009). RelA/p65 functions to maintain cellular senescence by regulating genomic stability and DNA repair. *EMBO Rep.* **10**, 1272-1278. doi:10.1038/embor.2009.197

Wei, S. and Sedivy, J. M. (1999). Expression of catalytically active telomerase does not prevent premature senescence caused by overexpression of oncogenic Ha-Ras in normal human fibroblasts. *Cancer Res.* **59**, 1539-1543.

Weikum, E. R., Knuesel, M. T., Ortlund, E. A. and Yamamoto, K. R. (2017). Glucocorticoid receptor control of transcription: Precision and plasticity via allostery. *Nat. Rev. Mol. Cell Biol.* **18**, 159-174. doi:10.1038/nrm.2016.152

Woods, D., Parry, D., Cherwinski, H., Bosch, E., Lees, E. and McMahon, M. (1997). Raf-induced proliferation or cell cycle arrest is determined by the level of Raf activity with arrest mediated by p21Cip1. *Mol. Cell. Biol.* **17**, 5598-5611. doi:10.1128/MCB.17.9.5598

Young, A. R. J., Narita, M., Ferreira, M., Kirschner, K., Sadaie, M., Darot, J. F. J., Tavaré, S., Arakawa, S., Shimizu, S., Watt, F. M. et al. (2009). Autophagy mediates the mitotic senescence transition. *Genes Dev.* **23**, 798-803. doi:10.1101/gad.519709

Zhang, L., Huang, X., Zhu, X., Ge, S., Gilson, E., Jia, R., Ye, J. and Fan, X. (2016). Differential senescence capacities in meibomian gland carcinoma and basal cell carcinoma. *Int. J. Cancer* **138**, 1442-1452. doi:10.1002/ijc.29882

Zhu, J., Woods, D., McMahon, M. and Bishop, J. M. (1998). Senescence of human fibroblasts induced by oncogenic Raf. *Genes Dev.* **12**, 2997-3007. doi:10.1101/gad.12.19.2997